19th Brazilian Congress of Thermal Sciences and Engineering
November 6th–10th, 2022, Bento Gonçalves - RS - Brazil

ENCIT2022-0582 - NUMERICAL SIMULATION OF DROSS TRANSPORT IN HOT DIP GALVANIZING FLOW

Waleska Gonçalves dos Santos
Universidade do Estado do Rio de Janeiro
santos.waleska@posgraduacao.uerj.b
Marilia Garcia Diniz
Universidade do Estado do Rio de Janeiro
diniz@uerj.br
Daniel José Nahid Mansur Chalhub
daniel.chalhub@eng.uerj.br
Norberto Mangiavacchi
norberto.mangiavacchi@eng.uerj.br

Abstract. *Zinc-coated steel sheets have high efficiency in corrosion resistance - and Hot Dip Galvanizing is one of the most used industrial methods for obtaining this type of coating. Certain factors can cause the development of intermetallics known as dross particles (Zn-Al-Fe) during this process, which can affect the final coated processes. Through fluid dynamics research, this project intends to investigate possible dross production in steel sheets with coated surfaces in a continuous hot-dip galvanizing line. The fluid dynamic characteristics of the process were studied using the gridap.jl library, written in Julia programming language, with particular attention paid to flow conditions and dross particle paths in the snout. Results of simulations show that changes in operational parameters like the strip speed, snout inclination, bath temperature and composition, affect dross particles density and distribution in the bath, thus affecting the final quality of the material.*

Keywords: *Gridap, Zinc Bath, Snout, Dross, Hot-dip Galvanizing*

1. INTRODUCTION

The Hot Dip Galvanizing (HDG) process is the most common type of coating in the industry to protects steel against corrosive damage present in atmospheric medium and water and is a process of coating steel sheets with a thin metallic layer for to protect of the part against corrosion damage. This process is characterized by the immersion of a metal part in molten zinc (Zn), which has electrochemical potential lower than that of other metals, thus serving as a sacrifice element and being corroded instead of the principal part, or substrate. Zinc is also capable of protecting the substrate from minor damages, as the electrochemical conditions allow it to generate a corrosion product that can act to repair a damaged local barrier. This is due to an increase in the volume of the corrosion products which fill the barrier failure. During galvanizing, the iron (Fe) present in the steel reacts with the molten zinc to form layers of intermetallic coating that act as a physical barrier between the steel substrate and the corrosive environment (Bellini *et al.*, 2019).

This work proposes a study of the zinc path in the HDG process of steel sheets using computational fluid dynamics. A simplified two-dimensional model of the problem is considered. Gridap library, written in Julia programming language, is the proposed tool to obtain the solution.

2. THE HOT DIP GALVANIZING

Several authors (Bellini *et al.*, 2019; Kania *et al.*, 2020; Fei *et al.*, 2021) define this process as a technique of bathing the part in pure zinc molten at high temperatures. This element forms a protective barrier, as its electrochemical potential is lower than that of the substrate, serving as a sacrificial element. It is also capable of protecting it in the event of minor damage, as the electrochemical conditions presented allow it to generate a corrosion product that can act as a repair in the damaged local barrier. This is due to an increase in the volume of corrosion products, which fill the gap in the coating.

According to Kania *et al.* (2020), the molten zinc baths used today contain a purity level of 99.995%. Of these 0.005%

of remaining impurities, the main one, in quantity, is iron, which enters the bath as a result of the dissolution of the substrates present in the steel of the part to be galvanized, which reach the saturation point of the liquid.

2.1 Additives in zinc bath

The addition of chemical elements, called additives, to the bath promotes the improvement of the properties of the materials that undergo the galvanizing process. Kania *et al.* (2020) presents a list of the main criteria to be considered when choosing these additives, the main ones being:
The chemical composition of the base material;
The lowest possible loss generation in the process;
The size, shape and complexity of the part to be galvanized;
The application of the final part;
The risk of material rupture in the bath;
The importance of corrosion resistance in the end use of the part.
The most common elements to be added are aluminum (Al) and nickel (Ni). Despite this, other elements can also be included such as titanium (Ti). The main study in this article was the formation of the so-called inhibition layer (IL), composed of Fe_2Al_5, responsible for the barrier that delays the formation of fragile Fe-Zn compounds that form between the substrate and the molten zinc area. The formation of this layer occurs from the concentration of 0.2% Al by total weight. The thickness of the sample was increased, as was the length of time the part remained in the bath. Nucleation and grain growth occurred simultaneously. In addition to the concentration factor, other parameters such as chemical constituents, bath temperature, substrate composition material, Fe dissolution, diffusion of Fe and Al elements in the bath, as well as the reactions between these elements and between Fe and Zn, also affect the formation of this inhibition layer.

2.2 The dross and its characteristics

Mahinroosta and Allahverdi (2018) describe dross as a mixture of metallic and non-metallic materials (salt and oxide) formed when molten aluminum comes into contact with air on its outer surface, oxidation of this surface and forming a semi-solid layer.

The combination of Al-Fe-Zn intermetallics in the bath may indicate different types of dross. They are mainly found of the superficial type, the main being the $Fe_2Al_5Zn_x$ type, the so-called upper dross, or top dross and the $FeZn_7$ phase, or lower or bottom dross (Wang *et al.*, 2018). These particles impair the quality of the steel as they can stick to the coating, causing ripples on the surface of the material. The surface dross is usually thinned out, while the bottom dross is only removed when the system is shut down.

As for its content, dross can be classified into two categories illustrated in Fig. 1. The superior one (Al-Fe-Zn) has a high Al content (more than 50% by weight of total dross). Other names used for this category are upper, primary or rich dross, which generally have a compact or agglomerated form (Fig. 2a). It is mainly produced during the primary production of aluminum, as the raw material for smelting is pure aluminum ingot.

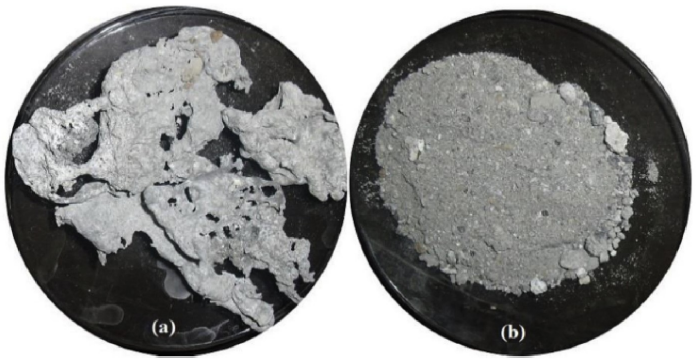

Figure 1. Dross classification: (a) upper (or primary) dross and (b) bottom (or secondary) dross. (Mahinroosta and Allahverdi, 2018)

The bottom dross (Zn-Fe), on the other hand, has a low Al content (between 5 and 20% in total weight) and is also known as secondary, dry or soft, and has a granular shape (Fig. 2b) . This dross has higher salt content and gas evolution than the primary. It is generated in secondary smelters, where the raw material is recycled aluminum itself. The differentiation between the types of dross is mainly due to their densities

2.3 Snout

The snout is a piece of metallic structure used to transfer the steel sheet to be galvanized from the oven to the molten zinc bath in the HDG process (Vieira *et al.*, 2022), and is described according to the schematic diagram of the Fig. 4.

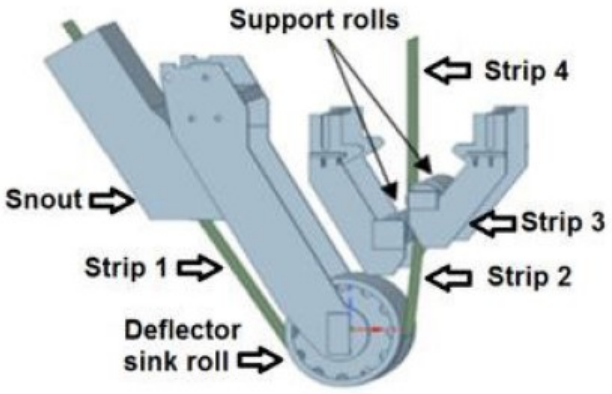

Figure 2. Schematic diagram of 1/5 scale snout operation. Adapted from (Vieira *et al.*, 2022)

The authors (Fei *et al.*, 2021) studied the effects of the production parameters and size of the flux fields and the appearance behavior of the bottom dross deposited in the zinc bath and the speed with which it passes through the bath.

3. COMPUTATIONAL FLUID DYNAMIC MODEL

In this work, the effect of the flow patterns on the occurrence of dross defects on the zinc coating on the upper surface of the steel strip will be addressed by numerical simulation of the fluid flow in the hot-dip galvanizing process. The chosen Computational Fluid Dynamic (CFD) model employed to simulate the fluid flow in the zinc bath was implemented using Gridap library (Badia and Verdugo, 2020).

Gridap provides a set of tools for the grid-based approximation of partial differential equations (PDEs) written in the Julia programming language. The library currently supports linear and nonlinear PDE systems for scalar and vector fields, single and multi-field problems, conforming and nonconforming finite element (FE) discretizations, on structured and unstructured meshes of simplices and n-cubes. Julia computer language (Bezanson *et al.*, 2012) features optional typing, multiple dispatch, and good performance, achieved using type inference and just-in-time (JIT) compilation, implemented using LLVM, a collection of modular and reusable compiler and tool chain technologies. It is multi-paradigm, combining features of imperative, functional, and object-oriented programming. Julia aims to create an unprecedented combination of ease-of-use, power, and efficiency in a single language. Additionally, it allows for easy access to high performance libraries written in C++, C, Fortran, and the rich set of libraries developed in Python. Thus, the utilization of Gridap, in combination of other high performance libraries in the Julia environment, allows for fast prototyping of applications, and provides tools to obtain high performance in scientific computing FEM applications.

The goal of the current work is to elucidate the basic physical phenomena involved in the hot-dip galvanizing process and, particularly, the role played by the flow patterns in the formation of dross inclusion defects on the coated surface. Therefore, several assumptions were made to simplify the model in order to obtain a preliminary understanding, that will be addressed in the following sections.

3.1 Model equations

The model equations are the steady-state, two-dimensional incompressible continuity and Navier-Stokes equations, which in non-dimensional *strong form* can be written as:

$$Re\,\mathbf{u}\cdot\nabla\mathbf{u}+\nabla p-\nabla\cdot\nabla\mathbf{u} = 0 \quad (1)$$

$$\nabla\cdot\mathbf{u} = 0 \quad (2)$$

where $\mathbf{u}$ is the flow velocity field, p is the pressure, and $Re=\frac{\rho UL}{\mu}$ is the Reynolds number, where U is the dimensional downward velocity of the strip, L is the bath depth, measured from the center of the sink roll to the surface of the bath, and μ is the dynamic viscosity. The non-dimensional radius of the sink roll is $R=0.4$, and the snout penetration depth is $d=0.1$ for the analyzed base case.The non-dimensional domain Ω is represented in Fig 4. The *weak form* is obtained by integrating over the domain Ω, with boundary Γ, the previous equations with appropriate weighting functions $\mathbf{v}$ and q, and applying Green's theorem, thus resulting in

$$\int_\Omega (\mathbf{v} \cdot Re\ (\mathbf{u} \cdot \nabla \mathbf{u}) + \mathbf{v} \cdot \nabla p + \nabla \mathbf{v} : \nabla \mathbf{u})\, d\Omega = \int_\Gamma \mathbf{v} \cdot (\mathbf{n} \cdot \nabla \mathbf{u})\, d\Gamma \quad (3)$$

$$\int_\Omega q\, \nabla \cdot \mathbf{u}\, d\Omega = 0 \quad (4)$$

3.2 Finite Elements Implementation

The approximation of problem 3-4 is performed employing inf-sub stable Lagrange polynomial elements with continuous velocities and discontinuous pressures (Elman *et al.*, 2014). The weak form associated to these interpolation spaces can be expressed as: find $(u, p) \in U_g \times Q_0$ such that $[r(u,p)](v,q) = 0$ for all $(v,q) \in V_0 \times Q_0$ where U_g and V_0 are the set of functions in V fulfilling the Dirichlet boundary condition g and 0 on $\partial\Omega$ respectively. The weak residual r evaluated at a given pair (u, p) is the linear form defined as

$$[r(u,p)](v,q) \doteq a((u,p),(v,q)) + [c(u)](v),$$

with

$$a((u,p),(v,q)) \doteq \int_\Omega \nabla v \cdot \nabla u\, \mathrm{d}\Omega - \int_\Omega (\nabla \cdot v)\, p\, \mathrm{d}\Omega + \int_\Omega q\, (\nabla \cdot u)\, \mathrm{d}\Omega, \quad (5)$$

$$[c(u)]\,(v) \doteq \int_\Omega v \cdot ((u \cdot \nabla)\, u)\ \mathrm{d}\Omega. \quad (6)$$

where the bilinear form a is associated with the linear part of the PDE, whereas c is the contribution to the residual resulting from the convective term.

In order to solve this nonlinear weak equation with a Newton-Raphson method, the Jacobian associated with the residual r is required. In this case, the Jacobian j evaluated at a pair (u, p) is the bilinear form defined as

$$[j(u,p)]((\delta u, \delta p),(v,q)) \doteq a((\delta u, \delta p),(v,q)) + [\mathrm{d}c(u)](\delta u, v), \quad (7)$$

where $\mathrm{d}c$ results from the linearization of the convective term, namely

$$[\mathrm{d}c(u)](\delta u, v) \doteq \int_\Omega v \cdot ((u \cdot \nabla)\, \delta u)\ \mathrm{d}\Omega + \int_\Omega v \cdot ((\delta u \cdot \nabla)\, u)\ \mathrm{d}\Omega. \quad (8)$$

The solution is obtained by applying a nonlinear PDEs solver in this multi-field FE problem. The implementation of this numerical scheme is done in Julia programming language, using the Gridap library (Badia and Verdugo, 2020), that supports both linear and non-linear PDE systems for scalar and vector fields. The Lagrange polynomials elements employed in the simulations are quadratic for the velocity and discontinuous linear for the pressure. The computation of the integrals restricted to each element is performed by Gaussian quadrature, and the nonlinear solver is based on the Newton-Raphson method.

4. RESULTS AND DISCUSSIONS

In order to capture the essence of the phenomena, a simplified two-dimensional model was implemented. The geometry was considered to be a perpendicular cross-section of the original scheme, in which only the fluid region between the strips and deflector roll was considered. Fig. 3 shows the computational domain with appropriate boundary conditions for the proposed model.

4.1 Mesh convergence verification

A convergence study, varying the mesh refinement, was performed to asses the correctness of the implementation and the accuracy of the simulations. A sequence of meshes, Case 1 to Case 8, with progressively higher level of refinement were generated employing Gmsh finite element mesh generator (Geuzaine and Remacle, 2009). A representative mesh is showed in Fig. 4, for the Case 4, with 2070 nodes and 4138 elements.

Table 1. summarizes the results of the convergence study of Cases 1-8, showing the values of the velocity components at a selected representative test point, with coordinates (-0.40,0.70) with respect to the center of the sink roll. The results show that grid Case 6, 7 and 8 have very small differences (less than 2%). Grid Case 6, with 30305 nodes and 60608 elements, was considered sufficiently refined for the present work, and is employed in the rest of the discussions.

To visualize the convergence of the solution we estimate the error of cases 1-7, using case 8 as best estimate of the correct solution. The result is plotted in Fig. 4. It can be observed that, asymptotically as $h \to 0$, the error decreases roughly as $O(h^2)$, showing a quadratic convergence.

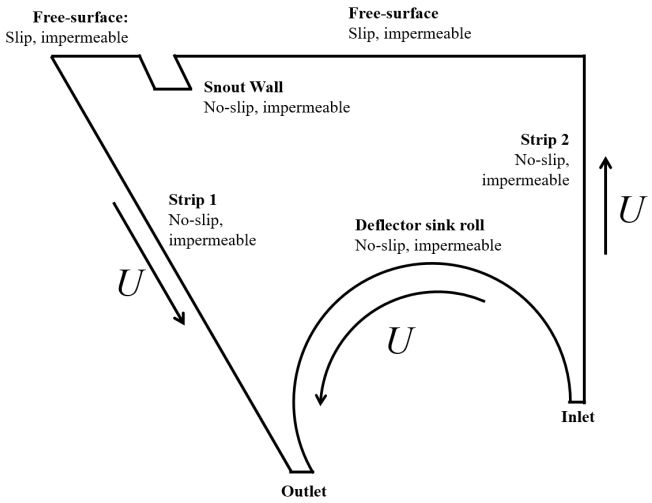

Figure 3. Computational domain with boundary conditions.

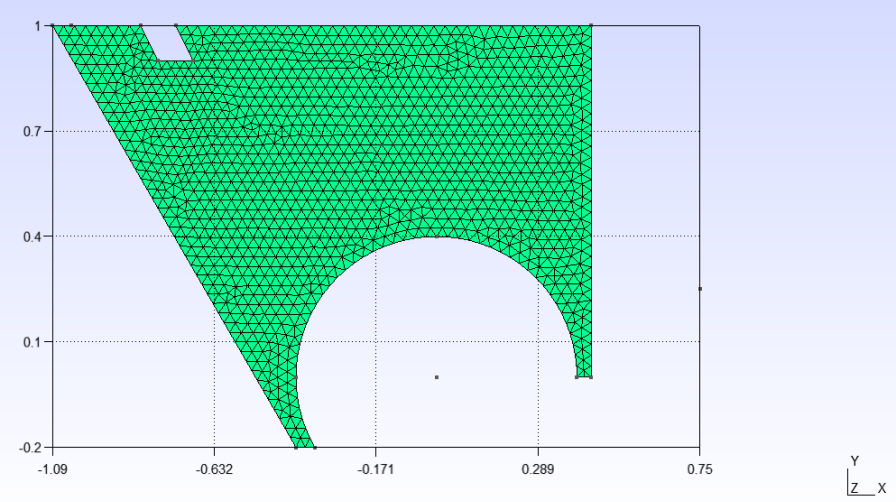

Figure 4. Domain Ω and example of mesh employed in the simulations: Case 4, with 2070 nodes and 4138 elements

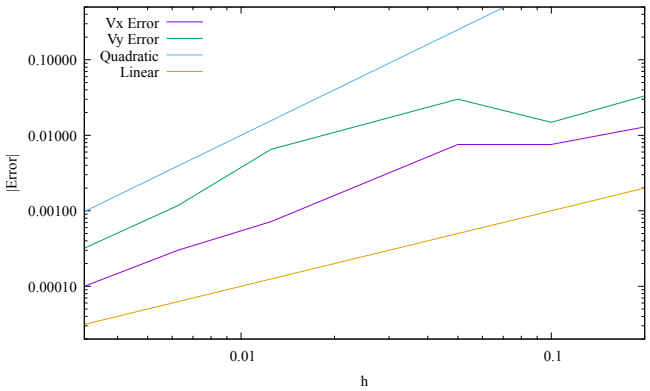

Figure 5. Estimated error in the velocity components at point $(-0.40, 0.70)$, for various h values.

4.2 Simulation results

The results of the Gridap simulations, using Case 6 mesh and $Re = 2000$, are presented in Fig. 6 to Fig. 8. The results obtained on the unstructured mesh are visualized employing Paraview (Ahrens *et al.*, 2005), an open-source, multi-platform data analysis and visualization application. They show the simulation of a tank with a zinc bath and a snout that is on top of the tank, and limited by a sink roll on the bottom. They represent the particle trajectories of an

Table 1. Convergence test for $Re = 50$. Velocity components at the point (-0.40,0.70), for grids with varying refinement levels.

Case	h	Nodes	Elements	Vx	Vy
1	0.200	62	122	0.034378892443111870	0.16049235577502874
2	0.100	180	358	0.029021107646983166	0.20851705156572536
3	0.050	585	1168	0.013897267738567764	0.16361133445116105
4	0.025	2070	4138	0.021152666819592155	0.17956662319937890
5	0.0125	7818	15634	0.020747711109047225	0.18717975007694546
6	0.00625	30305	60608	0.021766302971614990	0.19252755658144802
7	0.003125	119774	239546	0.021566789025353403	0.19337377108747683
8	0.0015625	475321	950636	0.021466711417017380	0.19369321535675868

idealized zinc bath, which considers a Newtonian fluid laminar flow in steady-state. These initial results were performed using a simplified two-dimensional geometric model, and using a null relative velocity between the particles and the fluid. A detailed study of the particle trajectories considering a more realistic geometry, buoyancy effects, turbulence models and inertia of the particles will be presented in future works.

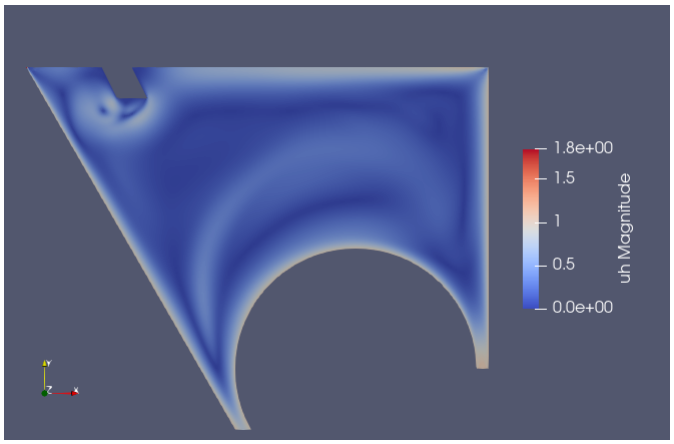

Figure 6. Velocity magnitude field obtained in the simulation, with Case 6 grid and Re=2000.

The velocity magnitude, presented in Fig. 6, shows the development of thin boundary layers on the surface of the descending strip, the sink roll surface, the ascending strip surface, and the free-surface. It is also observable a development of a jet projecting from the region where the descending strip is approaching the rotating cylinder.

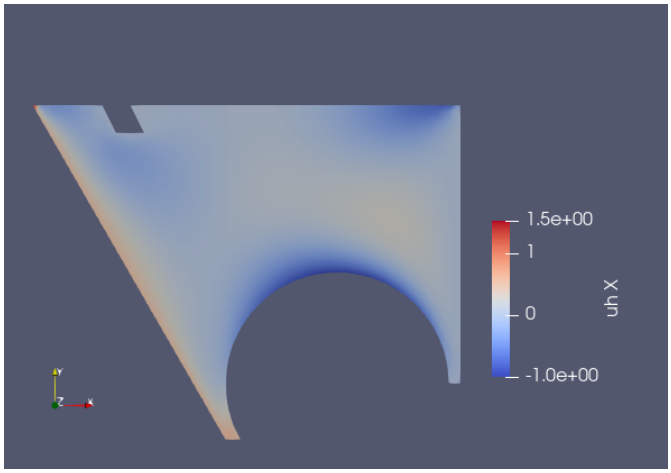

Figure 7. Velocity field, x-component, obtained in the simulation, with Case 6 grid and Re=2000.

The streamlines obtained in the simulations are summarized in Fig. 9 and show the formation of various re-circulation regions. On the left, the steel strip enters the bath and imparts a downward velocity to the flow. The bottom sink roll surface pushes flow against the descending strip on the left, thus causing the ejection of a liquid jet at approximately the

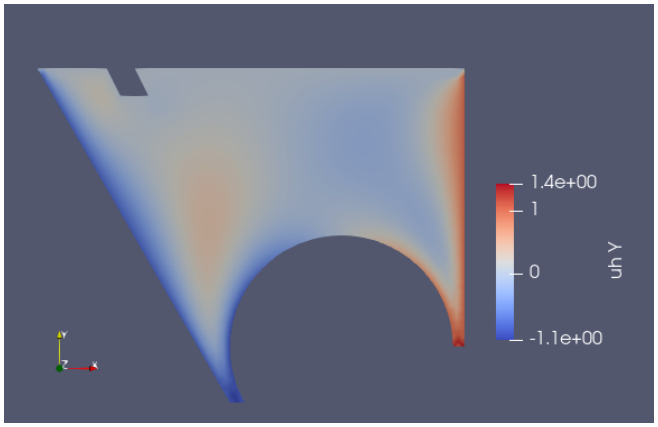

Figure 8. Velocity field, y-component, obtained in the simulation with Case 6 grid and Re=2000.

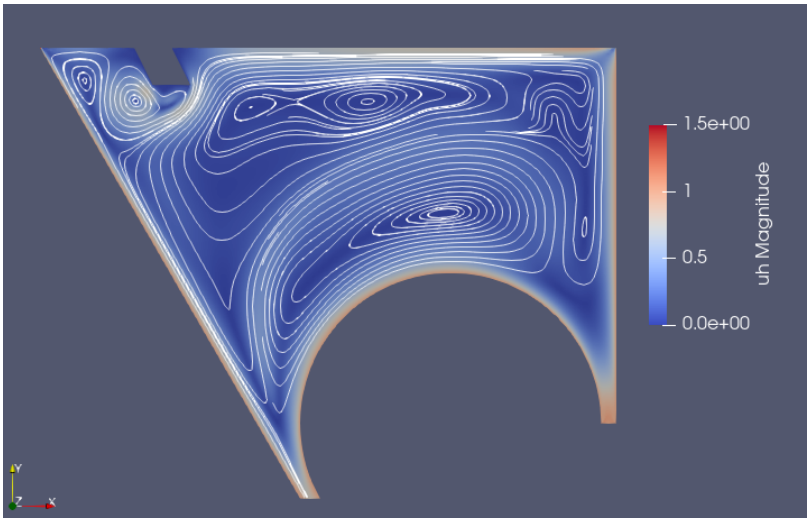

Figure 9. Streamlines, obtained in the simulation with Case 6 grid and Re=2000.

direction of the bisector angle. One large clockwise re-circulation region is formed above the cylinder interface, and is caused by the ejection of fluid from the region where the strip first approaches the cylinder, and the rotating sink roll action. Another large counterclockwise re-circulation is formed on the surface of the pool, thus dragging particles close to the surface towards the snout.

Most importantly, the downward movement of the strip induced the suction of liquid from the top of the bath down to the snout entrance and up to the snout internal meniscus.

Increasing the immersion of the snout, as shown in Fig. 10, shows a remarkable change in the fluid pattern in the region close to the entrance of the strip on the zinc bath.

Increasing the distance from the snout to the descending strip by $\Delta x = 0.1$, as shown in Fig. 10, also causes a strong modification on the fluid pattern in the region close to the entrance of the strip on the zinc bath, but also disrupts the recirculating flow above the sink roll. The fluid coming from the surface of the bath is deflected to a lower region of the downward moving strip, thus avoiding the entertainment of dross particles on the top left meniscus.

The simulations show that an accurate positioning of the snout can lead to an improved flow in the snout region, preventing the trapping of particles in the strip boundary layer.

5. CONCLUSIONS

This article presented a study of the continuous process of zinc bath hot-dip galvanization of steel sheets. The aim was to study possible dross formation in steel sheets with coated surfaces through fluid dynamics analysis. A simulation using the Gridap software was employed for the study of the fluid dynamic conditions of the process, addressing particularly the flow conditions and particle trajectories in the bath.

The behavior of ideal particles was achieved and could be observed using time evolution of particles and streamlines plot. Furthermore, initial results indicate that the flow pattern in the region inside the snout is likely to be one of the main issues leading to dross formation, due to possible accumulation of particles which get dragged and sucked by the

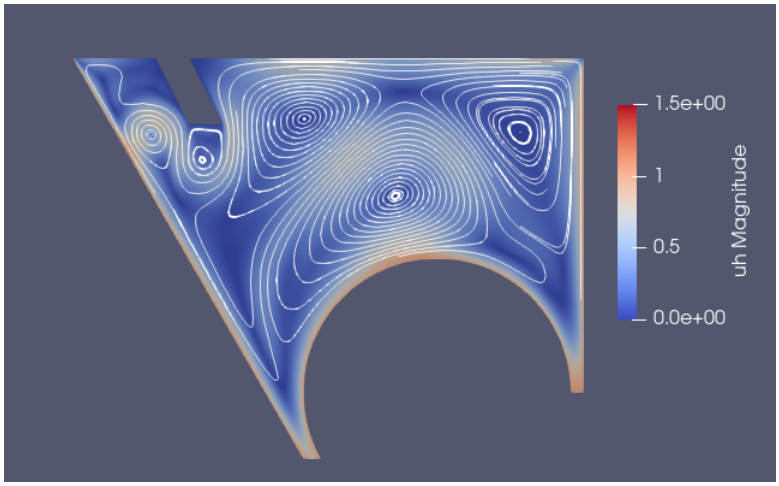

Figure 10. Streamlines, obtained in the simulation with Case 6 grid and Re=2000, modified to account for a deeper penetration of the snout in the bath. The depth of penetration of the snout in this case is increased by $\Delta y = 0.1$

.

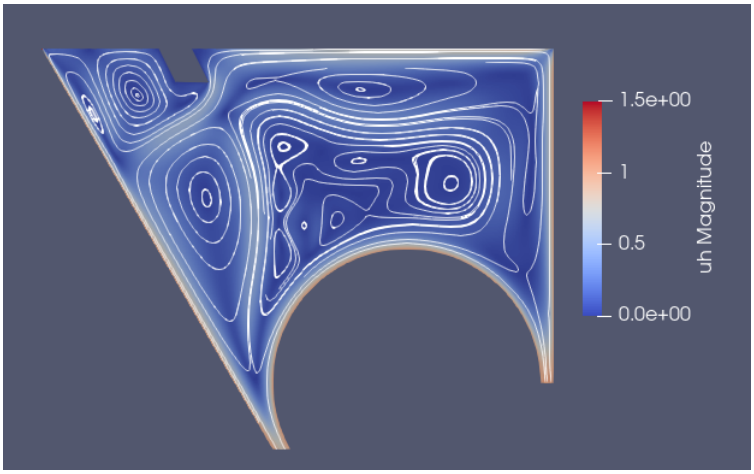

Figure 11. Streamlines, obtained in the simulation with Case 6 grid and Re=2000, modified to account for a displaced snout in the bath by $\Delta x = 0.1$.

downward motion of the strip, and get carried down in the boundary layer, and eventually are compressed by the sink roll against the strip. Hence, improving the positioning of the snout could potentially offer substantial opportunities for improvement in the quality of the final product. Although the implemented model was simplified, an interesting physical behavior could be observed leading to useful conclusions. Lastly, this is a preliminary work and future studies must be performed to confirm the results and obtain further conclusions.

6. ACKNOWLEDGEMENTS

The authors thank FAPERJ (Research Support Foundation of the State of Rio de Janeiro), CNPq (National Council for Scientific and Technological Research), and CAPES (Coordination for the Improvement of Higher Education Personnel) for their financial support.

7. REFERENCES

Ahrens, J., Geveci, B. and Law, C., 2005. "Paraview: An end-user tool for large data visualization". *The visualization handbook*, Vol. 717, No. 8.

Badia, S. and Verdugo, F., 2020. "Gridap: An extensible finite element toolbox in julia". *Journal of Open Source Software*, Vol. 5, No. 52, p. 2520. doi:10.21105/joss.02520. URL `https://doi.org/10.21105/joss.02520`.

Bellini, C., Iacoviello, F., Carlino, F. and Di Cocco, V., 2019. "The influence of hot dip galvanizing process on intermetallic phases formation". *Material Design & Processing Communications*, Vol. 1, No. 2, p. e39.

Bezanson, J., Karpinski, S., Shah, V.B. and Edelman, A., 2012. "Julia: A fast dynamic language for technical computing".

arXiv preprint arXiv:1209.5145.

Elman, H.C., Silvester, D.J. and Wathen, A.J., 2014. *Finite elements and fast iterative solvers: with applications in incompressible fluid dynamics*. Numerical Mathematics and Scie.

Fei, H., Li, J. and Li, H., 2021. "Size effect on flow field and dynamic deposition of bottom dross in a molten zinc pot". *ISIJ International*, Vol. 61, No. 5, pp. 1633–1640.

Geuzaine, C. and Remacle, J.F., 2009. "Gmsh: A 3-d finite element mesh generator with built-in pre-and post-processing facilities". *International journal for numerical methods in engineering*, Vol. 79, No. 11, pp. 1309–1331.

Kania, H., Mendala, J., Kozuba, J. and Saternus, M., 2020. "Development of bath chemical composition for batch hot-dip galvanizing—a review". *Materials*, Vol. 13, No. 18, p. 4168.

Mahinroosta, M. and Allahverdi, M., 2018. "Hazardous aluminum dross characterization and recycling strategies: A critical review." *Journal of Environmental Management*, Vol. 223, p. 452–468.

Vieira, R.R., Duarte, I.D., Eleutério, H.L., de Oliveira, T.G., Bagatini, M.C. and Tavares, R.P., 2022. "Trajectory of top-dross particles during the melting of zinc ingot in galvanizing pot". *Materials Research*, Vol. 25.

Wang, Z., Shi, J., Gao, A., Meng, L. and Guo, Z., 2018. "Recovery of zinc from galvanizing dross by a method of super-gravity separation." *Journal of Alloys and Compounds*, Vol. 735.

8. RESPONSIBILITY NOTICE

The authors are solely responsible for the printed material included in this paper.